Bioresource Technology 170 (2014) 76–82

Contents lists available at ScienceDirect

Bioresource Technology

journal homepage: www.elsevier.com/locate/biortech

Characterization of corncob-derived biochar and pyrolysis kinetics in comparison with corn stalk and sawdust

Xuan Liu, Yang Zhang, Zifu Li *, Rui Feng, Yaozhong Zhang

University of Science and Technology Beijing, Xueyuan Road 30, Beijing 100083, China

HIGHLIGHTS

- Characterization of corn cob was compared with corn stalk and sawdust.
- 16 reaction mechanisms were applied to deduce the corn cob pyrolysis mechanism.
- The kinetic parameters were calculated based on the best fitted mechanisms.
- The weight active energy of corn cob was lower than that of corn stalk and sawdust.

ARTICLE INFO

Article history:
Received 26 May 2014
Received in revised form 21 July 2014
Accepted 22 July 2014
Available online 1 August 2014

Keywords:
Corncob
Biochar
Pyrolysis
Thermo analysis
Kinetics

ABSTRACT

In this study, thermal and physicochemical characterization results of corncob (CC) and its derived biochars were analyzed and differentiated from sawdust (SD) and cornstalk (CS). The pyrolysis temperature shows the largest effect on the yield of biochar produced compare with residing time, heating rate, and feedstock particle size. The CC-derived biochars produced at temperatures ranging from 300 to 600 °C were analyzed. The CC was thermochemically altered to a stable biochar when the pyrolysis temperature was set to over 500 °C. To deduce the reaction mechanism of the CC during the major thermal decomposition stage, 16 mechanisms in solid-state reactions were applied. The reaction order and nucleation mechanisms described the thermal decomposition of the CC. By using the best-fitted mechanisms, the kinetic parameters were calculated. The weight active energy of the CC was 122.42 kJ/mol, which was the lowest value compared to those of CS and SD.

1. Introduction

Corn is one of the most extensively planted crops in the world. In China alone, the yield of corn reached 2.06×10^8 t in 2012 (China's National Bureau of Statistics, 2013). The ratio between corn grain and corncob (CC) may be about 100:18 (Cao et al., 2004), so approximately 3.7×10^7 t of CC could be generated in China every year. Cornstalk (CS) is usually kept on farmlands by corn harvesters. By contrast, the CC may collected, transported and separated together with the corn grain, and serve as a raw material in making low-grade fuels in many parts of the world. Therefore, proper processing and utilization of CC is important to yield economically important products.

Converting biomass via pyrolysis to produce quality products has become significant in recent years. Pyrolysis, one of the most commonly used thermochemical conversion technologies, involves thermal decomposition of organic components in an inert atmosphere at medium temperature to produce condensable and non-condensable components (including water, bio oil, and syngas) of biochar (Neves et al., 2011). Many studies are focusing on gas and liquid products that can be produced from corn residues through pyrolysis. These products are considered potential renewable energy sources, and the typical products are CO_2, CO, H_2O, CH_4, NH_3, acids, and aldehydes (CH_3COOH or furaldehyde) (Cao et al., 2004; Ioannidou et al., 2009). Renewable biomass, such as sawdust (SD) and CS, are highly recognized as valuable feedstock for biochar production due to their rich carbon compositions (Jahirul et al., 2012; Kamarudin et al., 2013; Lv et al., 2013). Meanwhile, the use of biochar as soil improver and as a medium in climate change mitigation strategy has gained much attention because biochar can be readily applied in soil to improve its productivity and fertility, can be used in carbon storage and sequestration, and can filter percolating soil water and its dissolved pollutants (Lehmann and Rondon, 2006; Roberts et al., 2010).

* Corresponding author. Tel./fax: +86 10 62334378.
E-mail address: zifulee@aliyun.com (Z. Li).

http://dx.doi.org/10.1016/j.biortech.2014.07.077
0960-8524/

However, studies on CC-derived biochar are limited. Yu et al. (Yu et al., 2010) discovered that microwave pyrolysis of CC leads to a stepwise accumulation of inorganic matter on exposed surfaces and some dissolved organic matter, resulting in the formation of cavities. Ioannidou et al. (Ioannidou et al., 2008) found that when CC was pyrolyzed at 800 °C for 1 h and underwent physical activation with steam at 800 °C for 15 min, the carbon products had the highest BET surface areas. The parameters of pyrolysis, such as temperature, residence time, heating rate, and feedstock particle size, can affect the quality and quantity of the produced biochar, and consequently, its interactions with the environment through application (Lehmann and Joseph, 2009).

Research on CC pyrolysis kinetics is limited. The function of the kinetic mechanism is a temperature-independent conversion that represents the reaction model, which depends on the actual kinetic mechanism. Notably, the application of first-order reaction models in biomass pyrolysis kinetics has become almost formulaic, and its indiscriminate acceptance has occurred without rigorous verification or sufficient awareness of its fundamental limitations (White et al., 2011; Xie et al., 2013). The imposition of an order-based model on a solid-state reaction system can cause a substantial divergence in the Arrhenius parameters (i.e., activation energies and pre-exponential factors). Inability to predict the kinetic behavior of biomass under different process conditions has vexed researchers and encouraged some of them to develop multiple-step models (White et al., 2011).

Given these reasons, this research was conducted to investigate the potential of CC as biochar feedstock. The effect of pyrolysis temperature, heating rate, residence time, and feedstock particle size in pyrolysis process to produce CC biochar products were studied. The characteristics of CC-derived biochars produced from 300 to 600 °C were analyzed. Meanwhile, 16 reaction mechanisms in solid-state reactions were applied, and the kinetic parameters were obtained. The physicochemical and thermochemical characteristics of CC, CS, and SD were analyzed and compared.

2. Methods

2.1. Biomass samples and their biochars

In this research, CC was chosen as feedstock. CS and SD were also analyzed for comparison. These biomasses were collected in a rural area in Henan Province of the middle eastern part of China. The feedstock were air dried and stored in sealed containers.

The lab-scale fixed bed reactor was used for slow pyrolysis. Pyrolysis was carried out in a reactor consisting of a quartz tube measuring 120 cm in length and 8 cm in diameter. The reactor was placed in an electrically heated horizontal oven. The sample was placed into a quartz holder, and then housed at the center of the tubular reactor. The sweep gas from a nitrogen cylinder at constant flow rate of 500 ml/min was precisely metered to the experimental system using a mass flow controller. In each test, 50 g sample was heated at room temperature to the setting temperature at a heating rate of 5, 10, 15 °C/min. The setting temperature was maintained for 40, 60, or 80 min to achieve a complete pyrolysis process. By the time the reactor has cooled down, the biochar was collected from the tube.

2.2. Analysis of biomass and biochar

The moisture content of the feedstock was estimated by measuring the weight loss after drying the fresh samples at 105 °C for 24 h. Ash contents were determined by the mass loss after burning the dried samples in a muffle furnace at 550 °C for 3 h. The volatile matter (VM) contents were determined based on the mass loss after heating the samples at 800 °C with the use of nitrogen for 20 min. The fixed carbon (FC) contents were calculated using the difference between the dry matter and the sum of the ash contents plus the VM contents (Azuara et al., 2013).

The elemental compositions (i.e., carbon, hydrogen, nitrogen, and sulfur) of the feedstock and produced biochars were determined using an elemental analyzer (Elementar, Germany). The oxygen value was calculated based on the result of the summation of the percentage of carbon, hydrogen, nitrogen, and sulfur subtracted from 100 (Ro et al., 2010).

The pH of each sample was determined from a mixture of 2 g of sample and 10 mL of deionized water following a 1 h equilibrium period.

The surface chemistry of the biochar was provided by a Nexus 670 Fourier transform infrared spectroscopy (FTIR) spectrophotometer (Thermo Nicolet Corporation, USA). The spectrum scope was recorded from 4000 to 400 cm^{-1} with a resolution of 4 cm^{-1}.

The BET surface area, which is a relative indicator of porosity in activated carbon, was determined using NOVA 4200e (Quantachrome, United States). All the resulting biochar samples were ground to pass through a 100-mesh sieve and degassed at 200 °C for 5 h to a residual pressure of approximately 10 mPa. Nitrogen (molecular cross-section of 0.162 nm^2) of 99.9% purity was used as adsorptive medium at 77 K. The micropore surface area was obtained from *t*-plot method.

The dried samples with average sample size of 10–30 mg were subjected to pyrolysis using Mettler–Toledo apparatus (United States), where the mass loss (thermogravimetry, TG) and mass loss rate (thermogravimetry derivative, DTG) were recorded simultaneously. All the samples were placed in an aluminum oxide (Al_2O_3) crucible with a lid and pyrolyzed using N_2 carrier gas at a flow rate of 20 mL/min at room temperature to 800 °C with a heating rate of 10 °C/min.

Van Soest analysis was carried out for raw fiber determination. The amounts of neutral detergent fiber (NDF), acid detergent fiber (ADF), acid detergent lignin (ADL), and ash contents were determined during sequential extraction in the ANKOM 220 fiber analyzer. The approximate contents of neutral detergent solubles (NDS), hemicellulose, cellulose, and lignin fractions were then calculated as the difference between starting weight and NDF, ADF and NDF, ADL and ADF, and ash and ADL, respectively.

To remove the effect of moisture and ash, the biochar yields were expressed into a dry ash free (daf) basis as follows:

$$Y_{\text{biochar, daf}}\ (\text{wt.}\%) = 100 \times (Y_{\text{biochar}} - A)/(100 - M - A)$$

$$Y_{\text{biochar, ad}}\ (\text{wt.}\%) = 100 \times \frac{M_{\text{biochar}}}{M_{\text{biomass}}}$$

where M_{biochar} (wt.%) represents the weight of biochar, $Y_{\text{biochar, ad}}$ (wt.%) represents the air-dried basis yields of biochar, and M and A (wt.%) are the moisture and ash contents of biomass, respectively.

2.3. Kinetic parameters of thermal degradation

The pyrolytic process of biomass could be represented by the following reaction scheme:

$$A(\text{biomass}) \rightarrow B(\text{biochar}) + C(\text{gas}) \quad (1)$$

The pyrolysis rate is defined as the equation of an Arrhenius type kinetic model as follows:

$$\frac{da}{dt} = k(T)f(a) \quad (2)$$

The advancement degree of reaction α could be derived from the TG curves

$$a = \frac{m_0 - m}{m_0 - m_\infty} \times 100\% \quad (3)$$

where m_0 represents the initial weight of the sample, m_∞ is the ending weight, and m is the remaining sample weight at time (t).

The rate constant k (T) is generally defined by the Arrhenius equation as follows:

$$k(T) = A \exp\left(-\frac{E}{RT}\right) \quad (4)$$

where E is the activation energy in J mol^{-1}, R is the gas constant in J K^{-1} mol^{-1}, A is the pre-exponential factor in s^{-1}, and T is the reaction temperature.

The combination of Eqs. (2) and (4) produces the following relationship:

$$\frac{da}{dt} = A \exp\left(-\frac{E}{RT}\right) f(a) \quad (5)$$

For a dynamic TG process, the heating rate β is as follows:

$$\beta = \frac{dT}{dt} \quad (6)$$

Introducing heating rate β to Eq. (5) results in the following:

$$\frac{da}{dT} = \frac{A}{\beta} \exp\left(-\frac{E}{RT}\right) f(a) \quad (7)$$

Eqs. (5) and (7) are the fundamental expressions of analytic methods to calculate the kinetic parameters based on TG data. Eq. (7) can be written in the following form:

$$\frac{1}{f(a)} da = \frac{A}{\beta} \exp\left(-\frac{E}{RT}\right) dT \quad (8)$$

Eq. (8) defines $G(\alpha)$ as

$$G(a) = \int \frac{1}{f(a)} da = \int \frac{A}{\beta} \exp\left(-\frac{E}{RT}\right) dT \quad (9)$$

As one of the most popular iso-conversional approaches, Coats–Redfern approximation (Gaia et al., 2013) was employed in this study, expressed as

$$\int \exp\left(-\frac{E}{RT}\right) dT = \left(\frac{RT^2}{E}\right) \exp\left(-\frac{E}{RT}\right) \quad (10)$$

By introducing Eq. (10) to Eq. (9), the reaction rate can be written in the following form:

$$\ln\left[\frac{G(a)}{T^2}\right] = \ln\left[\frac{AR}{\beta E}\left(1 - \frac{2RT}{E}\right)\right] - \frac{E}{RT} \quad (11)$$

In the temperature range of most thermal chemical reactions, $2RT$ is believed to be lesser than the majority of E (e.g., 60–300 kJ mol^{-1}). Therefore, $\ln\left[\frac{AR}{\beta E}\left(1 - \frac{2RT}{E}\right)\right]$ could be constant when the heat rate β is fixed. Hence, the kinetic of the biomass pyrolysis reaction can be tested with different $G(\alpha)$ through a linear correlation.

Meanwhile, in case of a zero-order reaction, $\ln\left(\frac{a}{T^2}\right)$ and $1/T$ demonstrate a linear relationship. Thus, activation energy (E) and frequency factor (A) can be determined from the slope and intercept of the straight line.

To achieve a comprehensive assessment of the apparent activation energy of the entire pyrolysis process for multi-step reactions, weighted apparent activation energy could be defined as

$$E' = \frac{\sum(E_n \times \theta_n)}{\sum \theta_n}, \quad (12)$$

where E_n and θ_n are the apparent activation energy and mass loss rate in every stage, respectively.

3. Results and discussion

3.1. Biomass characterization

Table 1 shows the comparison of the characteristics of air-dried samples. The proximate analysis results show that all three samples had high content of VM. The VM of CC was 69.5%, which is lower than that of SD (75.5%) but higher than that of CS (65.3%). VM exhibited the main mass loss in the pyrolysis process. The samples exhibited large variations in ash content. CC samples contained higher ash content (2.9%) than SD (1.2%) but much lower content than CS (11.7%). The ash content was mainly formed from soil and sand, which were mixed with biomass samples during the sample collection. The FC of CC (15.9%) was very close to that of CS (15.6%) but lower than that of SD (18.5%). Regardless of the ash and moisture contents, the VM/FC ratio showed that the VM in CC was higher than those of CS and SD, indicating that CC biochar yield may be lower than the other two samples (Lee et al., 2013).

Hemicellulose, cellulose, and lignin were the three main components of the used samples, although differences in their form rates were noted. The hemicelluloses in CC were about 1.4- and 1.8-fold those of CS and SD, whereas lignin was around 0.9- and 0.7-fold. These results may be related to the different components of plant residues. CCs are like seeds and fruits, which are composed of higher proteins, fats, and dietary fibers, among others. By contrast, SD and CS serve as the plant body containing more cellulose and lignin for structural support. Moreover, the neutral detergent solution content in CC was about twice those of SD and CS samples. This result also confirms the high protein and fat content of CCs.

3.2. The effect of the parameters of pyrolytic process on biochar yield

Taguchi method was used to analyze the effect of the parameters of the pyrolysis process on the biochar yield. The Taguchi method was developed to improve the implementation of total quality control. The effect of the factors on the properties and optimal conditions of factors can be determined using the Taguchi design. Determining the key factors and the optimal conditions based on the measured values of the characteristic properties is feasible (Wu et al., 2012). In this study, the biochar yield was selected because it results from the joint effects of temperature, heating rate, residence time, and feedstock particle size. The $L_9(3^4)$ table was used, and the parameters of the pyrolysis process are listed in Table 2.

The dependences of the yields of CC-derived biochars on the process parameters show that the difference between maximum

Table 1
Characterization of biomass samples.

Plant residue		CC	CS	SD
Proximate analysis (wt.%)	Moisture	11.7	8.4	9.9
	VM	69.5	65.3	70.4
	Ash	2.9	11.7	1.2
	FC	15.9	15.6	18.5
VM/FC		4.36	4.18	3.81
Ultimate analysis (wt.%)	C%	48.12	46.21	48.37
	H%	6.48	6.01	4.98
	O%	43.51	45.87	46.27
	N%	1.89	1.91	0.38
H/C		1.43	1.56	1.24
O/C		0.64	0.74	0.72
pH		6.4	7.1	7.2
Neutral detergent solution%[a]		9.5	5.5	4.1
Hemicelluloses%[a]		39.3	28.1	22.3
Cellulose%[a]		28.7	34.2	43.7
Lignin%[a]		19.6	21.7	28.8

[a] Dry ash free basis.

Table 2
The parameters of the pyrolysis process and CC-derived biochars yields.

No.	Pyrolysis temperature	Heating rate	Residence time	Feedstock particle size
1	(1) 400 °C	(1) 15 °C/min	(1) 30 min	(1) 2–4 mm
2	(1) 400 °C	(2) 10 °C/min	(2) 60 min	(2) 1–2 mm
3	(1) 400 °C	(3) 5 °C/min	(3) 90 min	(3)<1 mm
4	(2) 500 °C	(1) 15 °C/min	(2) 60 min	(3)<1 mm
5	(2) 500 °C	(2) 10 °C/min	(3) 90 min	(1) 2–4 mm
6	(2) 500 °C	(3) 5 °C/min	(1) 30 min	(2) 1–2 mm
7	(3) 600 °C	(1) 15 °C/min	(3) 90 min	(2) 1–2 mm
8	(3) 600 °C	(2) 10 °C/min	(1) 30 min	(3)<1 mm
9	(3) 600 °C	(3) 5 °C/min	(2) 60 min	(1) 2–4 mm
Level 1	30.80% ± 2.90%	26.60% ± 6.15%	26.77% ± 6.14%	26.27% ± 6.45%
Level 2	23.57% ± 0.91%	25.23% ± 4.84%	25.40% ± 4.70%	26.10% ± 4.16%
Level 3	22.37% ± 0.47%	24.90% ± 2.86%	24.57% ± 2.89%	24.37% ± 3.12%
R	8.43%	1.70%	2.20%	1.90%

and minimum values of the equal biochar yields (*R*) affected by the pyrolysis temperature was 8.43%, a value that is bigger than the residence time (2.20%), feedstock particle size (1.90%), and heating rate (1.70%). Higher reaction temperature led to lower biochar yield, which was due to a more thorough decomposition of organic components at higher temperature. This study suggests that pyrolysis temperature has the largest effect on the quality of biochar produced. Evidence shows that pyrolysis temperature may have a significant effect on biochar yield, pH, BET surface area, and carbon content (Agarwal et al., 2013; Lehmann and Joseph, 2009; Wang et al., 2013; Zhao et al., 2013a,b).

Compared with the pyrolysis temperature, the heating rate, residence time, and particle size did not substantially affect the biochar yield. However, the biochar yield produced at higher heating rate, shorter residence time, and bigger feedstock particle size were affected by the other three parameters at a more significant degree than the ones produced at a lower heating rate, longer residence time, and smaller feedstock particle size. For example, the standard deviation of the CC-biochar yield with a higher heating rate (15 °C/min) is as high as 6.15%, which is 2.15 times of that of lower heating rate (5 °C/min), the corresponding values of residence time and feedstock particle size are 2.13 and 2.07 times respectively. These results indicate that these parameters have an obvious influence on heat-transfer during the pyrolysis process (Agarwal et al., 2013; Ozyurtkan et al., 2008). Furthermore, a process with higher heating rate, shorter residence time, and bigger feedstock particle size was adverse to heat transfer during the pyrolysis process.

3.3. Characteristics of biochar produced at different temperatures

To evaluate the characteristics of the biochar produced at different temperatures, the CC-derived biochars were produced at pyrolysis temperatures of 300, 400, 500, and 600 °C, which were thereafter designated as CC300, CC400, CC500, and CC600. The pyrolysis temperature of 500 °C was selected as a baseline to differentiate the biochar properties exhibited by CCs, CSs, and SDs, which were designated as CC500, CS500, and SD500, respectively. The reason for selecting 500 °C for CS- and SD-derived biochars was that the key properties of the CS-derived biochars, such as pore structures and surface areas, were sufficiently developed at around 500 °C by complete thermal decomposition of cellulose and hemicellulose (Ioannidou et al., 2009; Lv et al., 2013). Meanwhile, the use of soil in growing corns in pots was effectively achieved by the biochar produced at 500 °C, although the effects of the different feedstock were more significant (Rajkovich et al., 2012). Several researchers have suggested that the reaction time should be set to 60 min for lignocellulosic-based feedstock (Ioannidou et al., 2009; Lehmann and Joseph, 2009; Stratford et al., 2014). Table 3 lists the properties of biochar produced at different temperatures and different feedstock using the aforementioned reactor.

From the proximate analysis, FC and ash contents of CC-derived biochars increased with pyrolytic temperature, whereas VM content significantly reduced from CC300 (43.6%) to CC500 (8.6%), and then dropped slightly to CC600 (7.2%). Meanwhile, the VM/FC ratio decreased significantly with an increase in temperature from 300 to 500 °C, but with a slight decline from 500 to 600 °C. These results corresponded to the main mass loss stage in the pyrolysis process.

The C, H, and O compositions of the samples and biochars were compared on a van Krevelen diagram, as shown in Fig. 1. Given the dissimilar O and H losses, atomic ratios varied as a function of feedstock type and pyrolysis temperature, where all molar ratios demonstrated a decreasing trend with increasing pyrolysis temperature (Cantrell et al., 2012). These trends were attributed to (1) removal of polar surface functional groups and (2) instances of higher degree of carbonization resulting in the formation of more aromatic structures that are more stable (Lehmann and Joseph, 2009).

The H/C ratios changed substantially with thermochemical treatment (Keiluweit et al., 2010). The H/C upper limit of 0.7 was used to distinguish biochars from biomass that have not been thermochemically altered from those that have been changed (International Biochar Initiative, 2012). In this study, the H/C ratios of all the three feedstock and CC300 were higher than 0.7, demonstrating that the pyrolysis time chosen in this study for biochar production was long enough to finish the thermochemical reaction. By contrast, the O/C ratios showed good correlation with the stability of biochars (Spokas, 2010). The O/C ratios of CC-derived biochars changed slightly when the pyrolysis temperature was higher than 500 °C, indicating that CC500 and CC600 have higher thermostability than CC300 and CC400. In addition, the H/C and O/C ratios of SD-derived biochars were lower than those of CC- and CS-derived biochars. These results demonstrated that SD samples had higher lignin content than CC and CS samples.

The major absorption bands representing the typical structure of CC-derived biochars were discern from the FTIR spectra. The characteristic bands located in 1429, 1464, 1509, and 1601 cm^{-1} indicate the existence of aromatic rings. The C—H bonds in CC300 and CC400 became weak in CC500 and almost disappeared in CC600. Moreover, the appearance of a carbonyl group between 1660 and 1675 cm^{-1} indicated that the C=O bond was in conjugation with the aromatic rings (Zhu et al., 2005). The absorption at 2927–2856 cm^{-1} corresponded to the C—H vibration of aliphatic carbons, and the absorption at 1437 cm^{-1} corresponded to the COOH bond (Wolbach and Anders, 1989), which almost disappeared in CC600. The O—H stretching in methyl groups was reflected in the band at 3408 cm^{-1} for each biochar sample.

The pH of CC-derived biochars increased with pyrolysis temperature, which tended to be more highly alkaline (pH 8.1–10.4)

Table 3
Summary of biochar properties.

Biochar		CC300	CC400	CC500	CC600	CS500	SD500
Proximate analysis (wt.%)	Moisture	2.4	2.1	1.6	1.7	1.8	1.2
	VM	43.6	20.8	8.6	7.2	8.9	13.1
	FC	49.1	71.7	81.6	82.4	76.6	80.6
	Ash	4.9	5.4	8.2	8.7	12.7	5.1
VM/FC		0.89	0.29	0.11	0.09	0.12	0.16
Ultimate analysis (wt.%)	C%	67.21	79.65	83.27	84.31	77.34	87.61
	H%	4.49	3.96	3.33	2.41	2.64	2.15
	O%	27.63	15.72	12.62	12.52	17.23	9.31
	N%	0.67	0.67	0.78	0.76	2.79	0.93
O/C		0.31	0.15	0.11	0.11	0.17	0.08
H/C		0.8	0.6	0.48	0.34	0.41	0.29
pH		8.1	9.1	9.3	10.4	10.1	9.5
Biochar yield (%)		77.3	36.9	23.3	21.7	30.9	22.6
BET (m^2/g)		61.8	180.1	212.6	192.9	201.3	243.1

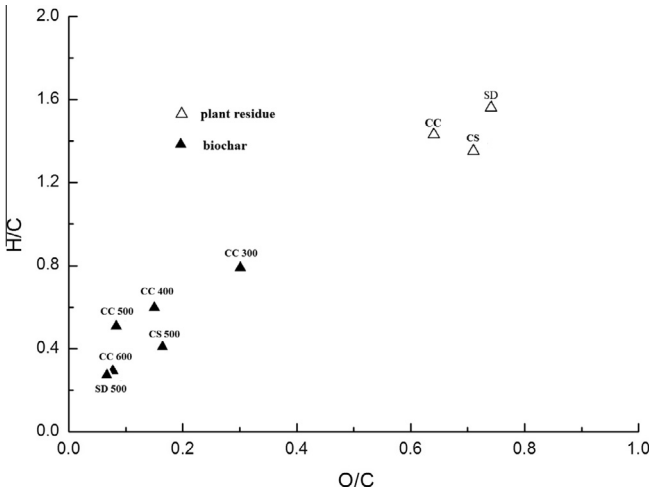

Fig. 1. H/C and O/C ratios for biomass and biochars (van Krevelen diagram).

compared with the feedstock. The alkalinity of biochar was influenced by organic functional groups and inorganic alkali. The contribution of organic functional groups such as —COOH and —OH decreased with increasing pyrolysis temperature with the progress of thermal decomposition, whereas the contribution of inorganic alkali such as Na and K became significant at a temperature higher than 500 °C (Lee et al., 2013). CC500 had a lower pH compared with CS500. Low concentrations of ash exhibited by lesser alkali and alkali-earth elements (Na, K, Ca, and Mg) could be the main reason for the stated results.

The BET surface area of CC-derived biochars increased significantly with increase in temperature from 300 to 500 °C, but slightly decreased at 600 °C. This finding can be attributed to polymerization reaction, which showed that microporous pores were destroyed in the resulting biochars (Neves et al., 2011). By contrast, the BET surface area of CC500 was lower than that of SD500 but higher than that of CS500. Higher surface areas of SD biochars have been reported previously, and the high ash content in CS may affect the formation of microporous structure.

3.4. TG–DTG curves

The TG results show that the biomasses possessed different pyrolysis characteristics, but the main mass loss ranges of their pyrolysis reactions were relatively low (about 200–500 °C). The mass loss temperature for CC-derived samples (~445 °C) may be lower than those of the CS- (~500 °C) and SD-derived samples (~700 °C). The maximum weight loss rate temperature of the SD-derived sample (~325 °C) was higher than those of the CC- and CS-derived samples (~285 °C). The reason for this result may be the fact that hemicellulose, cellulose, and lignin are the main polymer constituents of all the samples, but their chemical structures and corresponding thermal stabilities are different. Additionally, compositions proportions varied widely between biomass types and parts.

Based on the DTG curves, the pyrolysis process could be divided into three stages. The first stage (drying stage) with a slight mass loss of about 10% took place from 50 to 150 °C, which conformed to the extraction of moisture in the biomass samples. The second stage (pyrolytic decomposition stage) was aligned with the main part of mass loss. The mass loss ranges of the studied samples were within the temperature range 200–500 °C. Within this range, a pyrolytic thermal decomposition of cellulose and hemicellulose took place in the reactor. The primary volatiles produced from the thermal scission of chemical bonds comprised noncondensable gases (e.g., CO_2, CO, and CH_4) and condensable gases at ambient conditions (several organic compounds and water) (Neves et al., 2011). The third stage (carbonization stage) was due to the condensation reaction and further thermal decomposition of solid residues like chars and inorganic matter.

The pyrolytic decomposition stage was the main mass loss stage, where over 80% mass loss took place. Two reactions indicated two major decomposition mechanisms. The low-temperature stage of decomposition showed rapid mass decrease because of the volatilization of easy pyrolysis materials, whereas the high-temperature stage became slow in mass reduction due to the decomposition of lignin and intermediate products (Lv et al., 2010). Several organic compounds, such as cellulose and hemicellulose, decomposed at temperatures lower than 400 °C, most of which were translated into light-molecular weight compounds released as pyrolytic vapors (Xie et al., 2013). Moreover, the ash content in CS-derived samples was higher than those in CC- and SD-derived samples. The ash content was mainly formed by inorganic matter such as silicate, calcium carbonate, and potassium salts. A previous report has stated that mineral elements such as potassium salts had effects on the reduction of pyrolytic temperature (Liu et al., 2008; Zhao et al., 2013a,b). Furthermore, the TG/DTG results clearly show that the pyrolysis temperature of 500 °C, which was chosen in this study for biochar production, was high enough for differentiating the representative properties among the biochar samples.

3.5. Kinetic parameters of thermal degradation

As the CC pyrolysis process showed two stages of significant mass losses, the pyrolysis process could be divided into two stages in this study: the low-temperature stage (203–325 °C)and the high-temperature stage (325–457 °C). The expressions for the most common reaction mechanisms in solid-state reactions (Gaia

et al., 2013; Ozyurtkan et al., 2008; White et al., 2011) are shown in Table 4. Adopting the mentioned method, the linear regression rate (r^2) of CC pyrolysis is listed in Table 4 and the fit curves are shown in Fig. 2. The calculated apparent activation energy and weighted activation energy based on the fittest solid-state reaction are listed in Table 5.

Based on the results in Table 4, the reaction order and nucleation mechanisms described the thermal decomposition of CC well because the correlation coefficients (r^2s) in both stages were higher than the other values obtained from mampel, contracting geometry, and diffusional mechanisms. Meanwhile, the high value of r^2 from the linear regression analysis confirmed that the CC pyrolysis process was a thermochemical reaction with different stages.

Among the three models of reaction order, the second order model (F2, $r^2 = 0.9977$, the line in Fig. 2a) is the most probable mechanism for the low-temperature stage of CC pyrolysis because it has the best fitting accuracy. A similar conclusion was obtained from a previous research (Gaia et al., 2013) that suggested that the F2 model was the most probable mechanism function for the thermal decomposition of *Spirulina platensis*. The heat- and mass-transfer limitations may be the reasons for the stated phenomenon. Among the four models of nucleation, the Avrami–Erofeev model (A4, $r^2 = 0.9712$, the line in Fig. 2b) is the most probable mechanism for the high-temperature stage of CC pyrolysis. This finding means that the mechanisms of the high-temperature stage are random nucleation and nuclei growth. This conclusion also indicates that the carbonaceous content that formed in the low-temperature stage and the inorganic salt residue can induce the heterogeneous nucleation of the VM (Wang et al., 2006).

Based on the above-mentioned mechanisms, the kinetic parameters for CC pyrolysis are shown in Table 5. The results show that the E of CC was lower than those of CS and SD. E represents the minimum energy required to start a reaction. This study suggests that the CC pyrolysis process requires less energy than the other two plant residues, and works best for thermal treatment. The results revealed that CC contains more fats, proteins, and sugars than CS and SD, which are easier to decompose thermally compared with lignocellulose. Although the compositions of CC and CS were different, their Es shared some similarities to some extent,

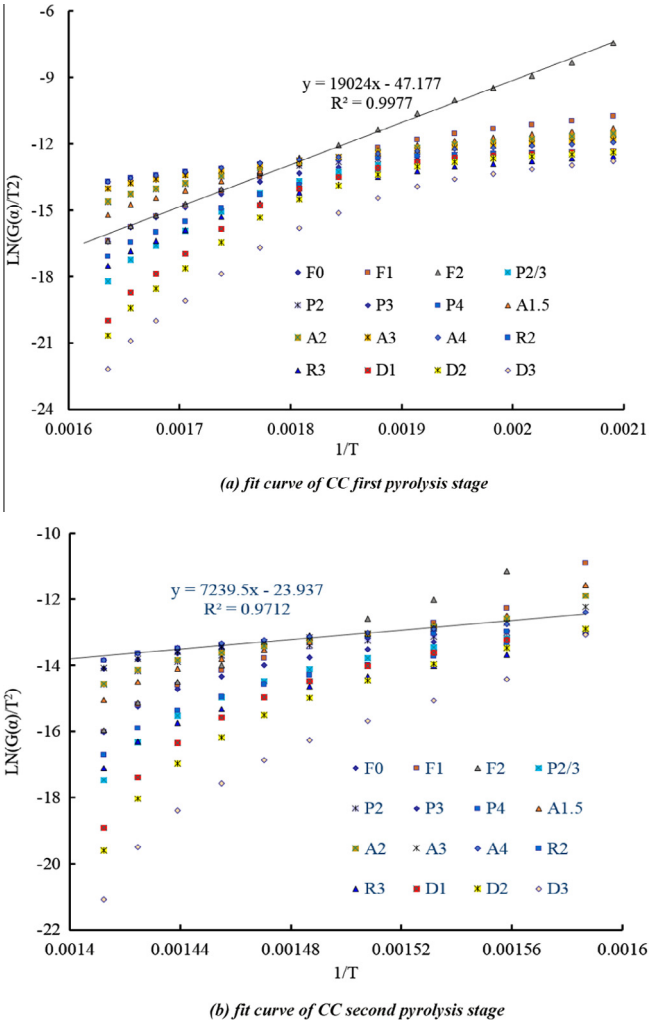

Fig. 2. Fit curve of CC pyrolysis process with different reaction mechanisms.

Table 4
Expressions for the most common reaction mechanisms in solid-state reactions and the linear regression rate of CC pyrolysis process.

Symbol	Reaction mechanisms	$f(\alpha)$	$G(\alpha)$	r^2_{low} [a]	r^2_{high} [b]
Reaction order					
F0	Zero-order	1	α	0.8507	0.8726
F1	First-order	$1-\alpha$	$-\ln(1-\alpha)$	0.9448	0.9619
F2	Second-order	$(1-\alpha)2$	$(1-\alpha)^{-1}-1$	0.9977	0.8348
Mampel					
P(2/3)	Power law	$2/3\alpha^{-1/2}$	$\alpha^{3/2}$	0.8402	0.8665
P2	Power law	$2\alpha^{1/2}$	$\alpha^{1/2}$	0.8767	0.8886
P3	Power law	$3\alpha^{2/3}$	$\alpha^{1/3}$	0.8963	0.9019
P4	Power law	$4\alpha^{3/4}$	$\alpha^{1/4}$	0.9115	0.9129
Nucleation					
A1.5	Avrami-Erofeev	$1.5(1-\alpha)[-\ln(1-\alpha)]^{1/3}$	$[-\ln(1-\alpha)]^{2/3}$	0.9486	0.9638
A2	Avrami-Erofeev	$2(1-\alpha)[-\ln(1-\alpha)]^{1/2}$	$[-\ln(1-\alpha)]^{1/2}$	0.9519	0.9655
A3	Avrami-Erofeev	$3(1-\alpha)[-\ln(1-\alpha)]^{2/3}$	$[-\ln(1-\alpha)]^{1/3}$	0.9577	0.9685
A4	Avrami-Erofeev	$4(1-\alpha)[-\ln(1-\alpha)]^{3/4}$	$[-\ln(1-\alpha)]^{1/4}$	0.9624	0.9712
Contracting geometry					
R2	Contracting cylinder	$2(1-\alpha)^{1/2}$	$1-(1-\alpha)^{1/2}$	0.9110	0.9271
R3	Contracting sphere	$3(1-\alpha)^{2/3}$	$1-(1-\alpha)^{1/3}$	0.9250	0.9443
Diffusional					
D1	One-dimensional diffusion	$1/(2\alpha)$	α^2	0.8585	0.8632
D2	Two-dimensional diffusion	$[-\ln(1-\alpha)]^{-1}$	$(1-\alpha)\ln(1-\alpha)+\alpha$	0.8839	0.8969
D3	Three-dimensional diffusion	$3/2(1-\alpha)^{2/3}[1-(1-\alpha)^{1/3}]^{-1}$	$[1-(1-\alpha)^{1/3}]^2$	0.9186	0.941

[a] The r^2 for low temperature stage of CC pyrolysis process.
[b] The r^2 for high temperature stage of CC pyrolysis process.

Table 5
Pyrolysis kinetic parameters for thermal decomposition of biomass.

Plant residue	Temperate range (°C)	Mass loss (%)	Mechanism model	E (kJ mol^{-1})	E' (kJ mol^{-1})	r^2
CC	203–325	57.8	F2	158.16	122.42	0.9977
	325–457	33.2	A4	60.19		0.9712
CS	210–318	52.6	F2	183.75	155.13	0.9935
	318–461	30.7	F1	106.10		0.9876
SD	225–375	77.9	F2	161.87	161.87	0.9741

i.e., activation energy value of low-temperature stage was higher than that of high-temperature stage, indicating that the heat transfer limitations may be the limiting step of the low-temperature stage in the CC and CS pyrolysis processes.

4. Conclusion

In this study, the thermal and physicochemical characterizations of CC and its derived biochars were analyzed and differentiated from those of CS and SD. The control factors on the biochar yield is the pyrolysis temperature. The H/C and O/C ratios showed that when the pyrolysis temperature is over 500 °C, the CC could be thermochemically changed to stable biochars. CC500 had the lowest pH compared to those of SD500 and CS500. The reaction order and nucleation mechanisms describe the CC pyrolysis reaction mechanism well. The CC-derived samples had the lowest E compared with those of the CS- and SD-derived samples.

Acknowledgement

This work was financially supported by the Fundamental Research Funds for the Central Universities (FRF-IC-11-001) of China.

References

Agarwal, M., Tardio, J., Mohan, S.V., 2013. Biohydrogen production from kitchen based vegetable waste: effect of pyrolysis temperature and time on catalysed and non-catalysed operation. Bioresour. Technol. 130, 502–509.
Azuara, M., Kersten, S.R.A., Kootstra, A.M.J., 2013. Recycling phosphorus by fast pyrolysis of pig manure: concentration and extraction of phosphorus combined with formation of value-added pyrolysis products. Biomass Bioenergy 49, 171–180.
Cantrell, K.B., Hunt, P.G., Uchimiya, M., Novak, J.M., Ro, K.S., 2012. Impact of pyrolysis temperature and manure source on physicochemical characteristics of biochar. Bioresour. Technol. 107, 419–428.
Cao, Q., Xie, K.C., Bao, W.R., Shen, S.G., 2004. Pyrolytic behavior of waste corn cob. Bioresour. Technol. 94, 83–89.
China's National Bureau of Statistics, 2013. China Statistical Yearbook 2013. China Statistical Press, Beijing.
Gaia, C., Zhang, Y., Chen, W., Zhang, P., Dong, Y., 2013. Thermogravimetric and kinetic analysis of thermal decomposition characteristics of low-lipid microalgae. Bioresour. Technol. 150, 139–148.
International Biochar Initiative, 2012. Standardized Product Definition and Product Testing Guidelines for Biochar That is Used in Soil. International Biochar Initiative.
Ioannidou, O., Zabaniotou, A., Antonakou, E.V., Papazisi, K.M., Lappas, A.A., Athanassiou, C., 2009. Investigating the potential for energy, fuel, materials and chemicals production from corn residues (cobs and stalks) by non-catalytic and catalytic pyrolysis in two reactor configurations. Renew. Sustain. Energy Rev. 13, 750–762.
Ioannidou, O.A., Stauropoulos, G.G., Zabaniotou, A.A., 2008. Use of biogenic solids for activated carbon via pyrolysis: the case of corn cob. High Temp. Mater. Process. (London) 27, 355–360.
Jahirul, M.I., Rasul, M.G., Chowdhury, A.A., Ashwath, N., 2012. Biofuels production through biomass pyrolysis – a technological review. Energies 5, 4952–5001.
Kamarudin, S.K., Shamsul, N.S., Ghani, J.A., Chia, S.K., Liew, H.S., Samsudin, A.S., 2013. Production of methanol from biomass waste via pyrolysis. Bioresour. Technol. 129, 463–468.
Keiluweit, M., Nico, P.S., Johnson, M.G., Kleber, M., 2010. Dynamic molecular structure of plant biomass-derived black carbon (biochar). Environ. Sci. Technol. 44, 1247–1253.
Lee, Y., Park, J., Ryu, C., Gang, K.S., Yang, W., Park, Y., Jung, J., Hyun, S., 2013. Comparison of biochar properties from biomass residues produced by slow pyrolysis at 500 °C. Bioresour. Technol. 148, 196–201.
Lehmann, J., Joseph, S., 2009. Biochar for Environmental Management: Science and Technology. Earthscan LLC, London.
Lehmann, J., Rondon, M., 2006. Bio-char soil management on highly weathered soils in the humid tropics. Biological approaches to sustainable soil systems. CRC Press, Boca Raton, 517–530.
Liu, Q., Wang, S., Luo, Z., Cen, K., 2008. Catalysis mechanism study of potassium salts on cellulose pyrolysis by using TG-FTIR analysis. J. Chem. Eng. Jpn. 41, 1133–1142.
Lv, D., Xu, M., Liu, X., Zhan, Z., Li, Z., Yao, H., 2010. Effect of cellulose, lignin, alkali and alkaline earth metallic species on biomass pyrolysis and gasification. Fuel Process. Technol. 91, 903–909.
Lv, G.J., Wu, S.B., Yang, G.H., Chen, J.C., Liu, Y., Kong, F.G., 2013. Comparative study of pyrolysis behaviors of corn stalk and its three components. J. Anal. Appl. Pyrol. 104, 185–193.
Neves, D., Thunman, H., Matos, A., Tarelho, L., Gomez-Barea, A., 2011. Characterization and prediction of biomass pyrolysis products. Prog. Energy Combust. Sci. 37, 611–630.
Ozyurtkan, M.H., Ozcimen, D., Mericboyu, A.E., 2008. Investigation of the carbonization behavior of hybrid poplar. Fuel Process. Technol. 89, 858–863.
Rajkovich, S., Enders, A., Hanley, K., Hyland, C., Zimmerman, A.R., Lehmann, J., 2012. Corn growth and nitrogen nutrition after additions of biochars with varying properties to a temperate soil. Biol. Fertil. Soils, 271–284.
Ro, K.S., Cantrell, K.B., Hunt, P.G., 2010. High-temperature pyrolysis of blended animal manures for producing renewable energy and value-added biochar. Ind. Eng. Chem. Res. 49, 10125–10131.
Roberts, K.G., Gloy, B.A., Joseph, S., Scott, N.R., Lehmann, J., 2010. Life cycle assessment of biochar systems: estimating the energetic, economic, and climate change potential. Environ. Sci. Technol. 44, 827–833.
Spokas, K.A., 2010. Review of the stability of biochar in soils: predictability of O:C molar ratios. Carbon Manage. 1, 289–303.
Stratford, J.P., Hutchings, T.R., de Leij, F.A.A.M., 2014. Intrinsic activation: the relationship between biomass inorganic content and porosity formation during pyrolysis. Bioresour. Technol. 159, 104–111.
Wang, D., Zhang, W., Hao, X., Zhou, D., 2013. Transport of biochar particles in saturated granular media: effects of pyrolysis temperature and particle size. Environ. Sci. Technol. 47, 821–828.
Wang, J., Wang, G., Zhang, M., Chen, M., Lib, D., Minc, F., Chen, M., Zhang, S., Ren, Z., Yan, Y., 2006. A comparative study of thermolysis characteristics and kinetics of seaweeds and fir wood. Process Biochem. 41, 1883–1886.
White, J.E., Catallo, W.J., Legendre, B.L., 2011. Biomass pyrolysis kinetics: a comparative critical review with relevant agricultural residue case studies. J. Anal. Appl. Pyrol. 91, 1–33.
Wolbach, W.S., Anders, E., 1989. Elemental carbon in sediments: determination and isotopic analysis in the presence of kerogen. Geochim. Cosmochim. Acta 53, 1637–1647.
Wu, X., Markham, J., Sun, X.S., Wang, D., 2012. Optimizing catalytic fast pyrolysis of biomass for hydrocarbon yield. Trans. ASABE 55, 1879–1885.
Xie, H., Yu, Q., Qin, Q., Zhang, H., Li, P., 2013. Study on pyrolysis characteristics and kinetics of biomass and its components. J. Renew. Sustain. Energy 5, 013122.
Yu, F., Steele, P.H., Ruan, R., 2010. Microwave pyrolysis of corn cob and characteristics of the pyrolytic chars. Energy Sources A Recover. Util. Environ. Eff. 32, 475–484.
Zhao, D., Dai, Y., Chen, K., Sun, Y., Yang, F., Chen, K., 2013a. Effect of potassium inorganic and organic salts on the pyrolysis kinetics of cigarette paper. J. Anal. Appl. Pyrol. 102, 114–123.
Zhao, L., Cao, X., Masek, O., Zimmerman, A., 2013b. Heterogeneity of biochar properties as a function of feedstock sources and production temperatures. J. Hazard. Mater. 256, 1–9.
Zhu, D., Kwon, S., Pignatello, J.J., 2005. Adsorption of single-ring organic compounds to wood charcoals prepared under different thermochemical conditions. Environ. Sci. Technol. 39, 3990–3998.